

*Quantum mushroom billiards*

Barnett, Alex H. and Betcke, Timo

2006

MIMS EPrint: **2006.387**

Manchester Institute for Mathematical Sciences  
School of Mathematics

The University of Manchester

Reports available from: <http://eprints.maths.manchester.ac.uk/>

And by contacting: The MIMS Secretary  
School of Mathematics  
The University of Manchester  
Manchester, M13 9PL, UK

ISSN 1749-9097

# Quantum mushroom billiards

Alex H. Barnett

*Department of Mathematics, Dartmouth College, Hanover, NH, 03755, USA\**

Timo Betcke

*Institut Computational Mathematics, TU Braunschweig, D-38023 Braunschweig, Germany†*

(Dated: October 12, 2006)

We report the first calculations of eigenmodes (quantum states) of a mushroom billiard of the type proposed by L. Bunimovich in this journal, **11**, 802 (2001). The phase space of this mixed system has a single regular region and a single ergodic region, and no KAM hierarchy. For a symmetric mushroom with a square foot, we find: i) low-eigenvalue modes with very high relative eigenvalue accuracy of order  $10^{-10}$ , and ii) high-eigenvalue modes at mode number around  $10^5$ . We outline the simple but highly-efficient mesh-free boundary collocation methods which make such calculations tractable. We test Percival’s conjecture that almost all modes localize either to regular or ergodic regions, report the relative frequencies of such modes, and examine Husimi distributions on the Poincaré surface of section.

Quantum chaos is the study of the quantum (wave) properties of Hamiltonian systems whose classical (ray) dynamics is chaotic. Billiards are some of the simplest and most studied examples; physically their waves analogs are vibrating membranes, or resonant quantum, electromagnetic, or acoustic cavities. Yet despite 150 years of study such wave resonance problems continue to provide a wealth of theoretical challenges. In particular ‘mixed’ systems, where the ray phase space has both regular and chaotic regions (the generic situation), are difficult to analyse. Five years ago Bunimovich described [1] a mushroom-shaped billiard whose mixed dynamics is free of the usual island hierarchies of Kolmogorov-Arnold-Moser (KAM). Its simplicity allowed a rigorous description of its dynamics. Bunimovich concluded by anticipating the *growth of “quantum mushrooms”*—it is precisely this gardening task that we achieve here. We use, and outline below, state-of-the-art, accurate and efficient numerical methods which compute eigenmodes using boundary information alone. Thus we are able to verify the conjecture of Percival [2] that in the high eigenvalue (short-wavelength) limit, modes live exclusively in invariant (regular or chaotic) phase space regions. We also show that these two mode types occur with a proportion given by their phase space volume ratio. We also show a multitude of pictures of modes in configuration space, on the boundary, and on the boundary phase space (the so-called Husimi function on the Poincaré surface of section).

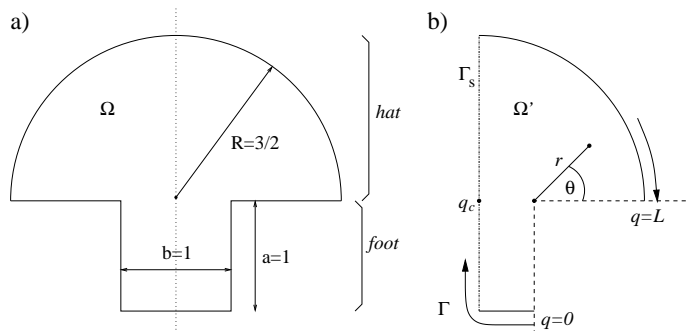


FIG. 1: Left: Mushroom billiard  $\Omega$  used in this work. The dotted line shows the reflection symmetry. Right: Desymmetrized half-mushroom domain  $\Omega'$  used for mode calculation, and polar coordinates. Dashed lines meeting at this corner are zeros enforced by basis functions. The remaining part of  $\partial\Omega'$  is  $\Gamma$ , comprising two pieces: Dirichlet boundary conditions on the parts shown as solid, while boundary conditions vary (see text) on the dash-dotted vertical line  $\Gamma_s$ . Boundary coordinate  $q \in [0, L]$  parametrizes  $\Gamma$ .

## I. INTRODUCTION

The nature of eigenfunctions of linear partial differential operators in the short wavelength, or semiclassical, limit remains a key open problem which continues to engage mathematicians and physicists alike. When the operator is the quantization of a classical Hamiltonian dynamical system, the behavior of eigenfunctions depends on the class of dynamics. In particular, hyperbolic dynamics (exponential sensitivity to initial conditions, or chaos) leads to irregular eigenfunctions, the study of which forms the heart of a field known as ‘quantum chaos’ [3] or ‘quantum ergodicity’ [4, 5]. The planar billiard, or free motion of a point particle trapped in a cavity  $\Omega \subset \mathbb{R}^2$  undergoing elastic reflections at the walls, forms one of the simplest examples since trajectories do not depend on overall energy, and the motion may be eas-

\*Electronic address: ahb(AT)math.dartmouth.edu

†Electronic address: t.betcke(AT)tu-bs.de

ily reduced to a one-dimensional area-preserving map on the boundary phase-space (*i.e.* locations and tangential velocities of collisions).

Billiards exhibit a menagerie of dynamical classes [6, 7, 8] ranging from complete integrability (ellipses and rectangles) to complete ergodicity (*e.g.* the stadium, known also to be mixing and Bernoulli [7]). Recently in this journal, Bunimovich introduced the so-called ‘mushroom’ billiard [1] with the novel feature of a well-understood divided phase-space comprising a single integrable (KAM) region and a single ergodic region. [49] As seen in Fig. 1a, the mushroom is the union of a half-disk (the ‘hat’) and a rectangle (the ‘foot’). Only trajectories reaching the foot are chaotic, thus as its width varies there is a continuous transition from integrability (the disk) to ergodicity (the stadium); for a review see [9]. The simplicity of its phase space allows detailed study of the general phenomenon of ‘stickiness’ (power-law decay of correlations) in the ergodic region [10, 11]. Bunimovich concludes by anticipating ‘quantum mushrooms’: this is the inspiration for our paper.

The quantum-mechanical system corresponding to billiards is the spectral problem of the Laplacian in  $\Omega$  with homogeneous boundary conditions (BCs). Choosing Dirichlet BCs (and units such that  $\hbar = 2m = 1$ ) we have

$$-\Delta\phi_j = E_j\phi_j \quad \text{in } \Omega, \quad (1)$$

$$\phi_j = 0 \quad \text{on } \partial\Omega. \quad (2)$$

This is known as the ‘drum problem’, and has a wealth of other applications to electromagnetic, optical, mechanical and acoustic resonance problems [12]. Eigenfunctions  $\phi_j$  (which we will refer to as eigenmodes, or simply modes) may be chosen real-valued and orthonormalized,

$$\langle\phi_i, \phi_j\rangle := \int_{\Omega} \phi_i(\mathbf{r})\phi_j(\mathbf{r})d\mathbf{r} = \delta_{ij}, \quad (3)$$

where  $d\mathbf{r} := dxdy$  is the usual area element. ‘Energy’ eigenvalues  $E_1 < E_2 \leq E_3 \leq \dots \rightarrow \infty$  may be written  $E_j = k_j^2$ , where the (eigen)wavenumber  $k_j$  is  $2\pi$  divided by the wavelength.

For domain shapes other than ellipses and rectangles (where separation of variables can be used to reduce it to a 1D problem), a fully 2D numerical computation is required to find modes and eigenvalues. Traditional methods employing finite differences or finite elements can handle a variety of shapes but have two major flaws: i) it is very cumbersome to achieve high convergence rates and high accuracy, and ii) they scale poorly as the eigenvalue grows. To illustrate the latter point, at eigenvalue  $E$  of order  $E^{1/2}$  wavelengths span the system size, and since several nodes are needed per wavelength, of order  $E$  degrees of freedom are needed in a finite element basis. The resulting difficulty of short-wavelength numerical calculation of eigenmodes is highlighted by the fact that analog computation with microwave cavities is still a popular

method in awkward geometries [13, 14]. In order to compute mushroom eigenmodes we use mesh-free boundary collocation methods which i) achieve exponential convergence (spectral accuracy), allowing eigenvalue computations approaching machine precision, and ii) require only of order  $E^{1/2}$  degrees of freedom (a feature shared by more standard boundary integral methods [15]). Furthermore at high eigenvalue we use an acceleration technique (the scaling method [16, 17, 18]) which results in another speed gain of order  $E^{1/2}$ . These improvements allow us to find large numbers of modes up to  $E \approx 5 \times 10^5$ .

Our goal in this paper is to compute eigenmodes of a mushroom billiard, at both low (Sec. III) and high eigenvalue (Sec. V), and provide some basic analysis of their properties, in particular their boundary functions (Sec. IV). We are motivated by a growing interest in quantum ergodicity [19, 20]. For ergodic dynamics, the Quantum Ergodicity Theorem [21, 22, 23, 24] (QET) states that in the  $E \rightarrow \infty$  (semiclassical) limit almost all modes become equidistributed (in coordinate space, also microlocally in phase space, and on the boundary [25, 26]). Since the mushroom phase space is divided, this theorem cannot be applied. However it is a long-standing conjecture of Percival [2] that for such mixed systems, modes tend to localize to one or another invariant region of phase space, with frequency in proportion to the phase space volumes, and that those in ergodic regions are equidistributed. Recently such a conjecture has been proven for certain piecewise linear quantum maps [27]. No rigorous results exist for billiards, although numerical work has been done in a smooth oval billiard [28]. We test this numerically for the mushroom in Sec. V, and show some computed Husimi (microlocal) distributions of high-eigenvalue modes on a Poincaré surface of section (a subset of the boundary).

With this goal in mind we first proceed by outlining and advertising our accurate and efficient numerical techniques for computing modes (Section II), with the hope that other researchers will use these tools to push beyond this preliminary study. Those interested purely in results should skip to Sec. III.

## II. NUMERICAL METHODS

### A. The Method of Particular Solutions

Our task is to compute Dirichlet eigenmodes of a domain  $\Omega$ . Mesh-based methods (finite elements, etc) typically use approximating functions that satisfy the boundary conditions (BCs) but not the partial differential equation (1). In contrast, we use a global approximation method where this situation is reversed: our set of basis functions, or *particular solutions*,  $\{\xi_m(\mathbf{r})\}_{m=1\dots M}$  satisfy the Helmholtz equation

$$-\Delta\xi_m = E\xi_m \quad (4)$$

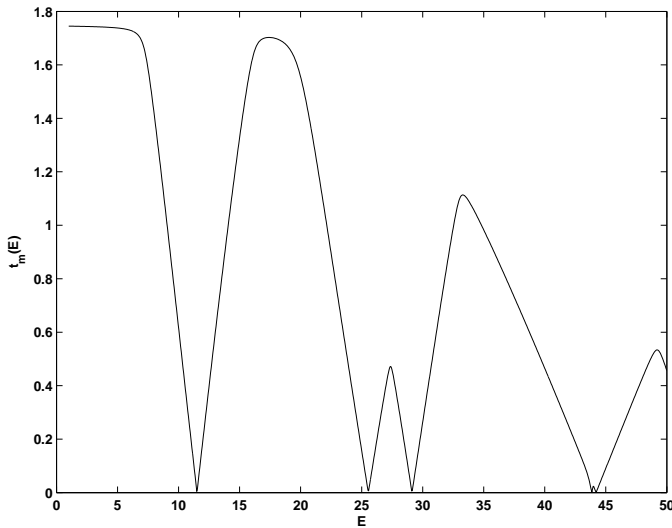


FIG. 2: The tension  $t_m(E)$  plotted as a function of trial eigenvalue parameter  $E$ . The minima indicate the eigenvalues of this domain. Close to  $E = 44$  there is a cluster of two eigenvalues. The half mushroom with zero Dirichlet boundary conditions was used (see Sec. II B).

at some trial eigenvalue parameter  $E$ , but do not individually satisfy (2). The goal is now to find values of  $E$  such that there exists nontrivial linear combinations  $x_1\xi_1 + x_2\xi_2 + \dots + x_M\xi_M$ , which are small on the boundary. These are then hopefully good approximations for an eigenfunction.

Let us make this precise. We define the space  $\mathcal{H}(E)$  of trial functions at a given parameter  $E$  as

$$\mathcal{H}(E) = \text{Span}\{\xi_1, \dots, \xi_M\}.$$

If we denote by  $\|u\|_{\partial\Omega}$  and  $\|u\|_{\Omega}$  the standard  $L^2$ -norm of a trial function  $u \in \mathcal{H}(E)$  on the boundary  $\partial\Omega$  and in the interior  $\Omega$  we can define the normalized boundary error (also called the tension) as

$$t[u] := \frac{\|u\|_{\partial\Omega}}{\|u\|_{\Omega}} \quad (5)$$

It is immediately clear that  $t[u] = 0$  for  $u \in \mathcal{H}(E)$  if and only if  $u$  is an eigenfunction and  $E$  the corresponding eigenvalue on the domain  $\Omega$ . However, in practice we will rarely achieve exactly  $t[u] = 0$ . We therefore define the smallest achievable error as  $t_m(E) = \min_{u \in \mathcal{H}(E)} t[u]$ . This value gives us directly a measure for the error of an eigenvalue approximation  $E$ , namely there exists an eigenvalue  $E_j$  such that

$$\frac{|E - E_j|}{E_j} \leq C t_m(E), \quad (6)$$

where  $C$  is an  $O(1)$  constant that only depends on the domain  $\Omega$ . This result is a consequence of error bounds

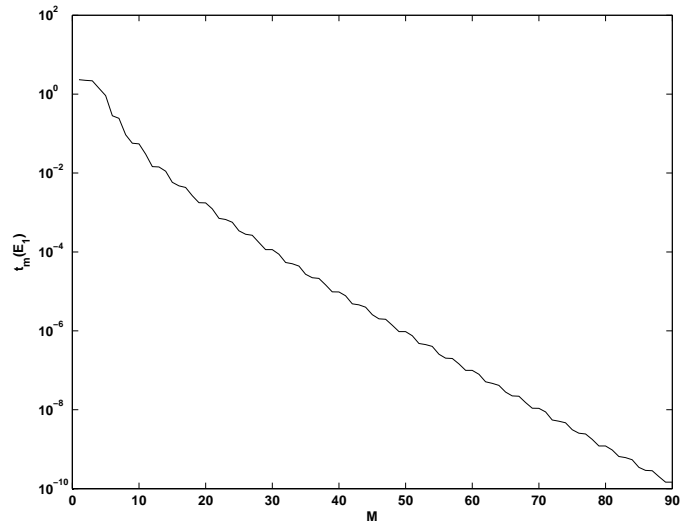


FIG. 3: Exponential convergence of  $t_m(E_1)$  with  $M$  the number of particular solutions used, for the first odd mode of the mushroom billiard. Here the eigenvalue parameter was held fixed at  $E_1$ , our best approximation to the eigenvalue (see Table Ia).

of Moler and Payne [29, 30]. Hence, by searching in  $E$  for minima of  $t_m(E)$  we find approximate eigenvalues with relative error given by a constant times  $t_m(E)$ . Fig. 2 shows such a plot of  $t_m(E)$  for our mushroom domain.

The implementation of this Method of Particular Solutions (MPS) depends on i) basis set choice, and ii) how to evaluate  $t_m(E)$ . The former we address in the next section. The latter requires a set of quadrature points  $\{\mathbf{y}_i\}_{i=1\dots N}$  on which to approximate the boundary integral  $\|u\|_{\partial\Omega}$ . One must take into account that Helmholtz basis sets tend to be ill-conditioned, that is, the  $N \times M$  matrix  $A$  with entries  $A_{im} := \xi_m(\mathbf{y}_i)$  becomes numerically rank-deficient for desirable choices of  $M$ . The tension  $t_m(E)$  can then be given by the square-root of the lowest generalized eigenvalue of the matrix pair  $(A^T A, B^T B)$ , or by the lowest generalized singular value of the pair  $(A, B)$ , where  $B$  is identical to  $A$  except with the replacement of  $\{\mathbf{y}_i\}$  by interior points [12, 17, 31]. These different approaches are discussed in [32]. Here, we use the generalized singular value implementation from [32], which is highly accurate and numerically stable. We note that these methods are related to, and improve upon, the plane wave method of Heller [33].

## B. Choice of basis functions

In order to obtain accurate eigenvalue and eigenfunction approximations from the MPS it is necessary to choose the right set of basis functions. In this section we propose a basis set that leads to exponential convergence, i.e. errors which scale as  $e^{-cM}$  for some  $c > 0$ , as

$M$  the number of basis functions grows.

To achieve this rate we first desymmetrize the problem. The mushroom shape  $\Omega$  is symmetric about a straight line going vertically through the center of the domain (see Fig. 1). All eigenmodes are either odd or even symmetric with respect to this axis. Hence, it is sufficient to consider only the right half,  $\Omega'$ . The odd modes are obtained by imposing zero Dirichlet boundary conditions everywhere on the boundary  $\partial\Omega'$  of the half mushroom. The even modes are obtained by imposing zero Neumann conditions on the symmetry axis  $\Gamma_s$  and zero Dirichlet conditions on the rest of  $\partial\Omega'$ .

Eigenfunctions of the Laplacian are analytic everywhere inside a domain except possibly at the boundary [34]. Eigenfunctions can be analytically extended by reflection at corners whose interior angle is an integer fraction of  $\pi$  [12]. The only singularity appears at the reentrant corner with angle  $3\pi/2$  (where dashed lines meet in Fig. 1b). Close to this corner any eigenfunction  $\phi_j$  can be expanded into a convergent series of Fourier-Bessel functions of the form

$$\phi_j(r, \theta) = \sum_{m=1}^{\infty} a_k J_{\frac{2m}{3}}(k_j r) \sin \frac{2m}{3} \theta, \quad (7)$$

where the polar coordinates  $(r, \theta)$  are chosen as in Fig. 1b. The function  $J_\alpha$  is the Bessel function of the first kind of order  $\alpha$ .

The expansion (7) suggests that the basis set  $\xi_m := J_{\frac{2m}{3}}(kr) \sin \frac{2m}{3} \theta$ , where  $k^2 = E$ , might be a good choice since these functions capture the singularity at the reentrant corner and automatically satisfy the zero boundary conditions on the segments adjacent to this corner (dashed lines in Fig. 1b). Hence, we only need to minimize the error on the remaining boundary  $\Gamma$  which excludes these segments. The boundary coordinate  $q \in [0, L]$  parametrizes  $\Gamma$ ; its arc length is  $L = 3(1 + \pi/4)$ . This Fourier-Bessel basis set was originally introduced by Fox, Henrici and Moler [35] for the L-shaped domain. In [36] the convergence properties of this basis set are investigated and it is shown that for modes with at most one corner singularity the rate of convergence is exponential.

In Fig. 3 we demonstrate the exponential convergence of  $t_m(E_1)$  for the eigenvalue  $E_1$  of the first odd-symmetric mode of the mushroom. We have  $t_m(E_1) = O(e^{-cM})$  for some  $c > 0$  as the number  $M$  of basis functions grows. Hence, for the minimum  $\hat{E}$  of  $t_m(E)$  in an interval containing  $E_1$  it follows from (6) that

$$\frac{|\hat{E} - E_1|}{E_1} \leq Ct_m(\hat{E}) \leq Ct_m(E_1) = O(e^{-cM}),$$

which shows the exponential convergence of the eigenvalue approximations  $\hat{E}$  to  $E_1$  for growing  $M$ .

### C. Scaling method at high eigenvalues

For all but the lowest modes we used an accelerated MPS variant which is much more efficient but less ac-

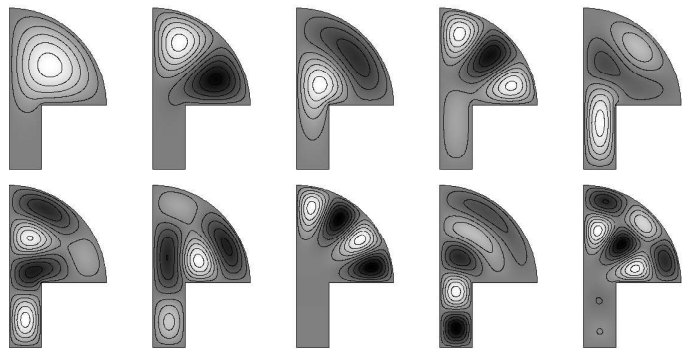


FIG. 4: The first 10 odd modes of the mushroom shape, shown as density plots. Eigenvalue increases rightwards from the top left. They are obtained by imposing zero Dirichlet boundary conditions on the symmetry axis. White corresponds to positive and black to negative values. Expressed as a fraction of  $\|\phi_j\|_{L^\infty(\Omega)}$ , the level curves range from  $-0.9$  to  $0.9$  with a spacing of  $0.2$ .

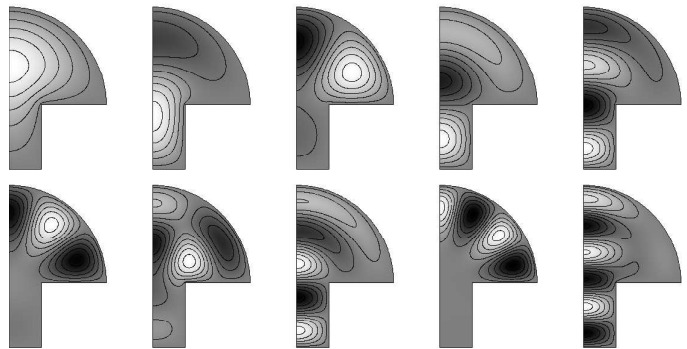


FIG. 5: The first 10 even modes of the mushroom shape, plotted as in the previous figure. They are obtained by imposing zero Neumann boundary conditions on the symmetry axis.

curate than the MPS. The *scaling method* [16, 17, 18] makes use of a basis of particular solutions; we used the above basis. To our knowledge the scaling method has not been applied to a re-entrant corner before. At large eigenvalues  $E > 10^3$ , rather than determine the basis size  $M$  by a convergence criterion as in Sec. II B, we use the Bessel function asymptotics: for large order  $J_\alpha(x)$  becomes exponentially small for  $x/\alpha < 1$  (the turning point is  $x = \alpha$ ). Equating the largest argument  $kR$  (with  $R = 3/2$ ) with the largest order  $2M/3$  gives our semiclassical basis size  $M \approx 9k/4$ .

Given a center wavenumber  $k_0$  and interval half-width  $\Delta k$ , the scaling method finds all modes  $\phi_j$  with  $k_j \in [k_0 - \Delta k, k_0 + \Delta k]$ . This is carried out by solving a single indefinite generalized eigenvalue problem involving a pair of matrices of the type  $A^T A$  discussed above. The ‘scaling’ requires a choice of origin; for technical reasons we are forced to choose the singular corner. Approximations to eigenvalues lying in the interval are related to

the matrix generalized eigenvalues, and the modes to the eigenvectors. The errors grow [17] as  $|k_j - k_0|^3$ , thus the interval width is determined by the accuracy desired; we used  $\Delta k = 0.1$  which ensured that  $t_m(E)$  errors associated with the modes rarely exceeded  $3 \times 10^{-4}$ . Since the search for minima required by the MPS has been avoided, and on average  $O(k)$  modes live in each interval, efficiency per mode is thus  $O(k) = O(E^{1/2})$  greater than the MPS. By choosing a sequence of center wavenumbers  $k_0$  separated by  $2\Delta k$ , all modes in a large interval may be computed.

We are confident that the scaling method finds all odd modes in a desired eigenvalue window. For instance we compute all 1746 odd symmetry modes with  $k_j < 100$ , using 500 applications of the scaling method (at  $k_0 = 0.1, 0.3, \dots, 499.9$ ). We verify in Fig. 7 that there appears to be zero mean fluctuation in the difference between the (odd) level-counting function  $N(k) := \#\{j : k_j \leq k\}$  and the first two terms of Weyl's law [3],

$$N_{\text{Weyl}}(k) = \frac{\text{vol}(\Omega')}{4\pi} k^2 - \frac{|\partial\Omega'|}{4\pi} k, \quad (8)$$

where  $|\partial\Omega'|$  is the full perimeter of the half mushroom domain. The scaling method is restricted to Dirichlet BCs only, hence we cannot find even symmetry modes this way. We note the method is still not well-understood from the numerical analysis standpoint [17, 18].

In applying the scaling method to the mushroom, the vast majority of computation time involves evaluating Bessel functions  $J_\alpha(x)$  for large non-integral  $\alpha$  and large  $x$ . This is especially true for producing 2D spatial plots of modes as in Fig. 10, for which of order  $10^9$  evaluations are needed. We currently use independent calls to the GSL library [37] for each  $J_\alpha(x)$  evaluation. This is quite slow, taking between 0.2 and 50  $\mu\text{s}$  per call (2.4GHz Opteron CPU, linux/GNU), with the slowest being in the region  $\alpha < 50$ ,  $10^2 < x < 10^3$ . However, we note that Steed's method [38, 39], which is what GSL uses in this slow region, is especially fast at evaluating sequences  $J_\alpha(x), J_{\alpha-1}(x), J_{\alpha-2}(x), \dots$ , and that since  $\alpha$  is a multiple of a rational with denominator 3, only 3 such sequences would be needed to evaluate all basis functions  $\{\xi_m(\mathbf{r})\}_{m=1\dots M}$  at a given location  $\mathbf{r}$ . We anticipate at least an order of magnitude speed gain could be achieved this way.

### III. LOW EIGENVALUE MODES

In this section we present results for the first few even and odd modes on the mushroom billiard. The odd modes are obtained by solving the eigenvalue problem with zero Dirichlet boundary conditions on the half mushroom shape from Fig. 1b, using the MPS, by locating minima in the tension function of Fig. 2. In Table Ia the eigenvalues are listed to at least 10 significant digits, and in Fig. 4 the corresponding modes are plotted. We emphasize that it is the exponentially convergent nature

a)	$j$	$E_j$	b)	$j$	$E_j$
	1	11.50790898		1	5.497868889
	2	25.55015254		2	13.36396253
	3	29.12467610		3	18.06778679
	4	43.85698300		4	20.80579368
	5	44.20899253		5	32.58992604
	6	53.05259777		6	34.19488964
	7	55.20011630		7	41.91198264
	8	66.42332921		8	47.37567140
	9	69.22576822		9	54.62497098
	10	82.01093712		10	65.18713235

TABLE I: Tables of a) lowest 10 odd and b) lowest 10 even eigenvalues of the mushroom. All digits shown are believed to be correct.

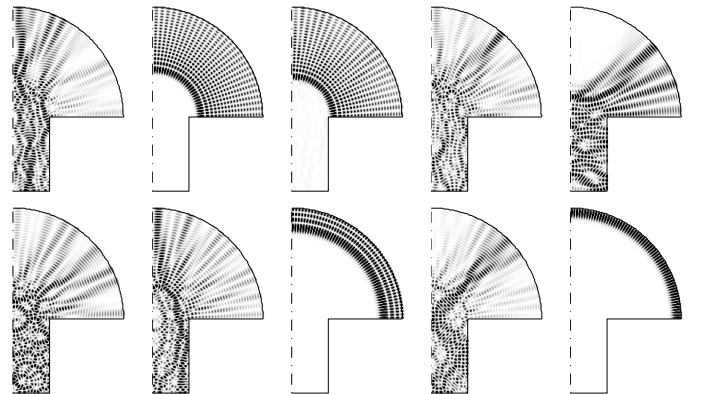


FIG. 6: The 10 odd modes of the mushroom whose eigenwavenumbers lie in the range  $90 < k_j < 90.35$ , at mode number about  $j \approx 8100$ . Intensity  $|\phi_j|^2$  is shown with zero white and larger values darker.

of our method that makes reaching such high accuracies a simple task.

As explained in Sec. II B the even modes require imposing Neumann BCs on  $\Gamma_s$  and Dirichlet BCs on the remaining part of  $\Gamma$ . This was achieved in the MPS by modifying the tension function (5) to read

$$t[u] := \frac{\left( \|\partial_n u\|_{\Gamma_s}^2 + \|u\|_{\Gamma \setminus \Gamma_s}^2 \right)^{1/2}}{\|u\|_{\Omega'}} \quad (9)$$

where the normal derivative operator on the boundary is  $\partial_n := \mathbf{n} \cdot \nabla$ , the unit normal being  $\mathbf{n}$ . Table Ib, gives the smallest 10 even modes on the mushroom billiard, and the corresponding modes are plotted in Fig. 5.

Although we are far below the semiclassical regime some odd and even functions already show properties of the underlying classical dynamical system. For example, the 8<sup>th</sup> odd and the 6<sup>th</sup> even mode live along a caustic and therefore show features of the classically integrable phase space while the 7<sup>th</sup> odd and 10<sup>th</sup> even mode already

shows features of the classically ergodic phase space. For comparison, in Fig. 6 we show some modes with intermediate eigenvalues of order  $10^4$  (mode number  $j = 8 \times 10^3$ ), and in Section V we will present high-lying modes around  $j = 4 \times 10^4$ . Here we plot the intensity  $|\phi_j|^2$  rather than  $\phi_j$  since at such short wavelengths this shows large-scale features better. In these cases it becomes clearly visible that in the semiclassical regime the modes of the mushroom either correspond to the integrable or to the ergodic regions of phase space.

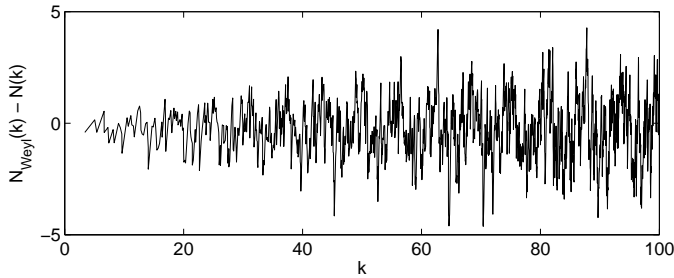


FIG. 7: Difference between the mode counting function  $N(k)$  and the two-term Weyl's prediction  $N_{\text{Weyl}}(k)$  defined by (8).

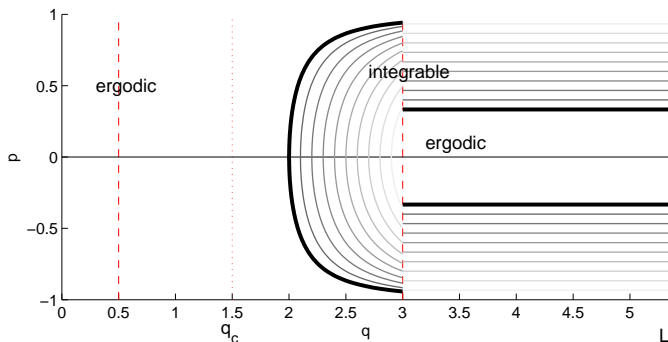


FIG. 8: Poincaré surface of section (PSOS), that is, the classical phase space in boundary coordinates  $q$  (as shown in Fig. 1b) and  $p$  (sin of incidence angle). Vertical dashed lines shows location of corners. The vertical dotted line shows location of  $q_c$  the focal point of the hat. The dark line shows the border of integrable phase space; note that  $q = 2$  corresponds to the smallest possible caustic for integrable phase space. Families of orbits defined by constant angular momentum are shown by lines in the integrable region. Note that they exchange vertical ordering at the corner, as indicated by their grayscale color labeling.

#### IV. BOUNDARY FUNCTIONS

We choose a Poincaré surface of section (PSOS) [3] defined by Birkhoff coordinates  $(q, p) \in \Gamma \times [-1, 1] =: Z$ , where  $q$  is the boundary location as before (see Fig. 1b)

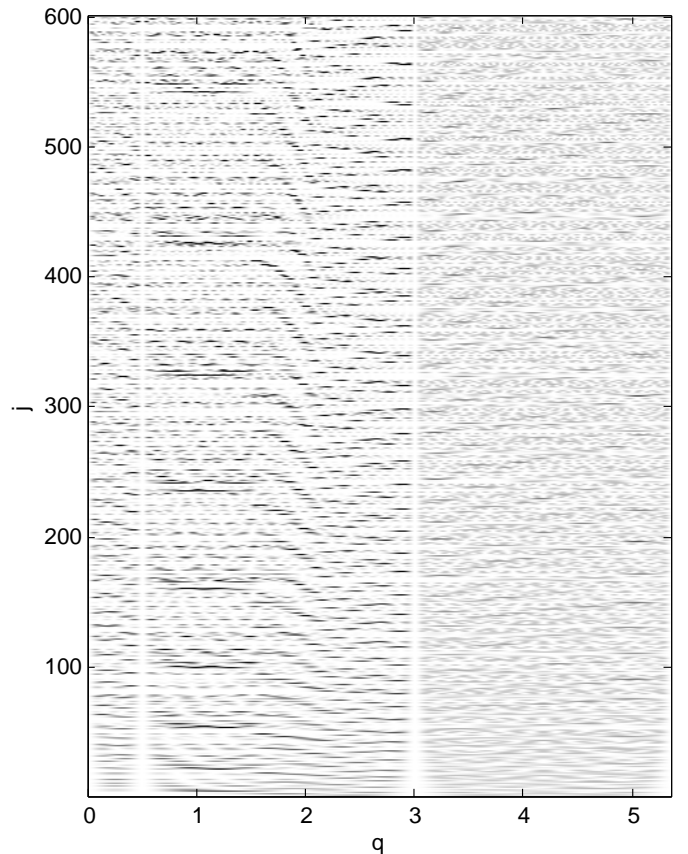


FIG. 9: Intensity of boundary normal-derivative functions  $|\partial_n \phi_j(q)/k_j|^2$ , plotted vs boundary coordinate  $q$  on the horizontal axis and mode number  $j \in [1, 600]$  on the vertical. The density plot shows white as zero, and larger values darker.

and  $p$  the tangential velocity component, in the clockwise sense, for a unit speed particle. (If the incident angle from the normal is  $\theta$  then  $p = \sin \theta$ ). The structure of this PSOS phase space is shown in Fig. 8. Our choice (which differs from that of Porter *et al.* [9]) is numerically convenient since it involves only the part of the boundary on which matching is done (Sec. II). Despite the fact that it does not cover the whole boundary  $\partial\Omega'$ , it is a valid PSOS since all trajectories must hit  $\Gamma$  within bounded time.

Integrable phase space consists of precisely the orbits which, for all time, remain in the hat [1] but which never come within a distance  $b/2$  from the center point  $q_c$ . This latter requirement is needed to exclude the zero-measure set of marginally-unstable periodic orbits (MUPOs) in the ergodic region which nevertheless remain in the the hat for all time [10, 11]. Simple geometry shows that the curved boundary between ergodic and integrable regions consists of points  $(q, p)$  satisfying

$$q - q_c = \frac{b/2}{\sqrt{1 - p^2}}, \quad \text{for } p^2 \leq p_0^2 := 1 - \frac{b^2}{4R^2}. \quad (10)$$

For our shape,  $q_c = a + b/2 = 3/2$ ,  $p_0^2 = 8/9$ . In the domain  $q \in [q_c + R, L]$  the boundary occurs at the lines  $p = \pm b/2R = \pm 1/3$ . Successive bounces that occur on  $\Gamma$  are described by the PSOS billiard map  $f : Z \rightarrow Z$ . Any such Poincaré map is symplectic and therefore area-preserving [3].

The quantum boundary functions  $\partial_n \phi_j(q)$  for  $q \in [0, L]$  are natural representations of the modes. They are convenient to work with at high eigenvalue because of their reduced dimensionality: compared to a 2D representation of  $\phi_j$  they are much faster to compute and require less storage (by factor  $O(k)$  in each case). Note that they are not  $L^2(\partial\Omega)$  normalized; rather they are normalized according to a geometrically-weighted  $L^2$  boundary norm via the Rellich formula (see [18, 40])

$$\int_{\partial\Omega} (\mathbf{r} \cdot \mathbf{n}) |\partial_n \phi_j|^2 dq = 2E_j, \quad (11)$$

where  $\mathbf{r}(q)$  is the location of boundary point  $q$  relative to an arbitrary fixed origin.

In Fig. 9 we show the first 600 odd-symmetry boundary functions. More precisely, intensities (squared values) are shown, divided by  $E_j$  so as to remove the overall scaling of their norm evident in (11). Several features are visible. Typical spatial frequencies increase with  $j$ . There is an absence of intensity near the corners (over a region whose size scales as the wavelength). The region  $3 < q < L$ , in which phase space is predominantly integrable, has a more uniform intensity than  $0 < q < 2$ , which is exclusively ergodic. The region  $2 < q < 3$  is almost exclusively integrable, but is dominated by classical turning-points corresponding to caustics; these appear as localized regions of high intensity with the form of an Airy function. In  $1/2 < q < 3/2$  there are horizontal bright streaks corresponding to horizontal ‘bouncing-ball’ modes (with various vertical quantum numbers) in the foot. An interesting feature in Fig. 9 is a series of slanted structures visible for  $3/2 < q < 2$ . These are fringes which move as a function of wavenumber, and we refer the reader to another publication for their analysis [41].

## V. HIGH EIGENVALUE MODES AND PERCIVAL’S CONJECTURE

In Fig. 13 we show a sequence of 20 modes with consecutive eigenvalues near wavenumber  $k = 500$  (eigenvalue  $E = 2.5 \times 10^5$ ). These modes are a subset of the modes produced via a single generalized matrix eigenvalue problem (of size  $M \approx 1200$ ) using the scaling method at  $k_0 = 500$ . The full set of 77 modes (including evaluating boundary functions) took 20 minutes to compute (2.4GHz Opteron CPU). Typical tension  $t_m(E)$  values were below  $10^{-3}$ . Naively applying (6) we would conclude only about 3 significant digits of accuracy on eigenvalues. However, it is possible to rigorously improve this bound by factor  $O(E_j^{1/2})$  [31], which in fact means we have about 6 significant digits. At short wavelength the

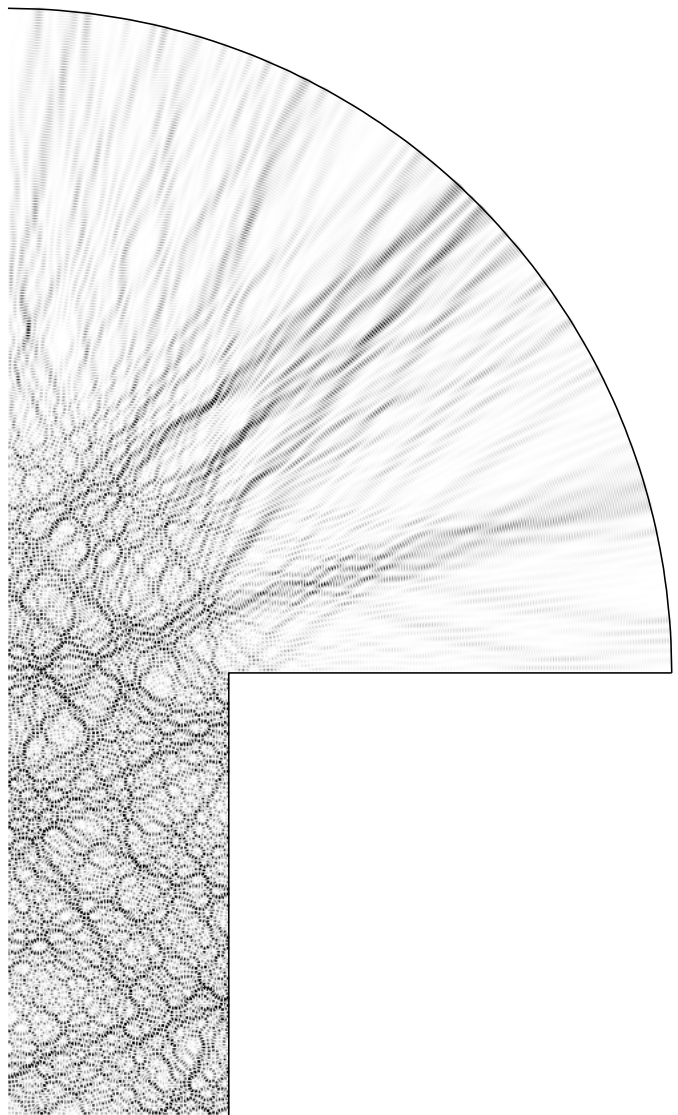


FIG. 10: High-energy eigenmode with  $k_j = 499.856 \dots$ , at around  $j \approx 45000$ . This mode appears to live in the ergodic region.

2D spatial plots such as Fig. 13 take much longer to compute than boundary functions; this figure took a couple of hours to produce. Fig. 10 shows the 14th in the sequence in more detail. Clearly in this small set, Percival’s conjecture seems to hold: modes are either regular or chaotic but not a mixture of both. We will now study this in more detail on the PSOS phase space.

### A. Husimi distributions of boundary functions

We define the Husimi transform [42] of functions on  $\mathbb{R}$ , for convenience reviewing the coherent state formalism in dimensionless ( $\hbar$ -free) units. Given a width parameter (phase space aspect-ratio)  $\sigma > 0$ , it is easy to show that

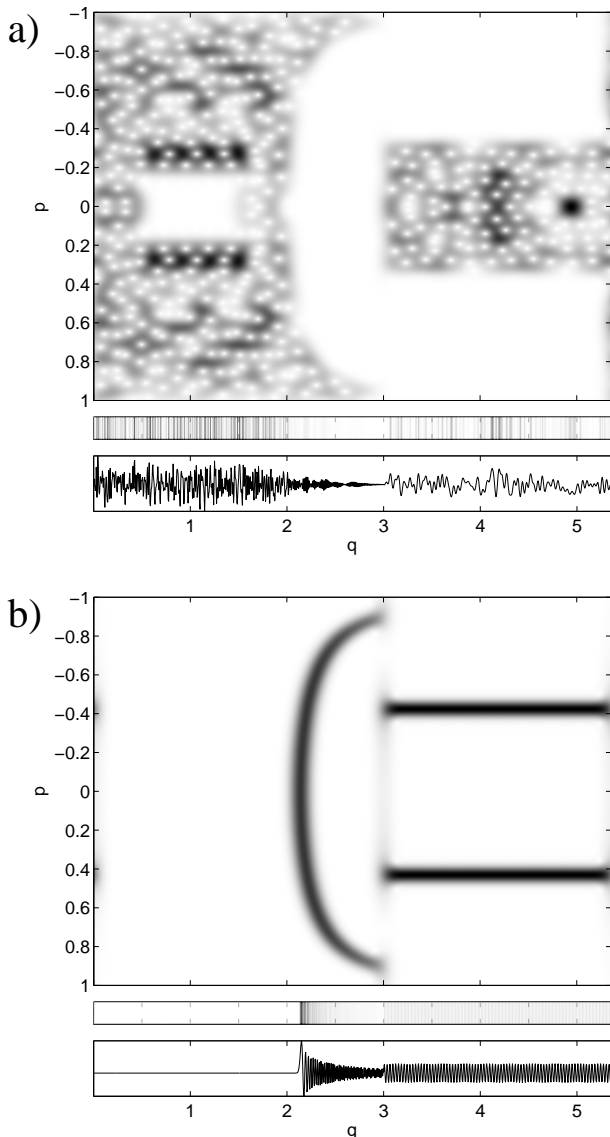


FIG. 11: a) the mode of Fig. 10 Husimi distribution  $H_{\partial_n \phi_j, \sigma}(q, p)$  defined by (15) (top), density plot of  $|\partial_n \phi_j|^2$  (middle), and graph of  $\partial_n \phi_j$  (bottom). Note the  $q$  coordinate is common to the three plots. b) Similar representation of the next highest mode at  $k_j = 499.858$ , the 15<sup>th</sup> in the sequence of Fig. 13, which lives in the regular region.

the annihilation operator

$$a := \frac{1}{\sqrt{2}} \left( \frac{q}{\sigma} + \sigma \partial_q \right) \quad (12)$$

has a kernel spanned by the  $L^2$ -normalized Gaussian  $\psi_0(q) := (\pi\sigma^2)^{-1/4} e^{-q^2/2\sigma^2}$ . We work in  $L^2(\mathbb{R})$ , in which the hermitian adjoint of  $a$  is  $a^\dagger = (q/\sigma - \sigma \partial_q)/\sqrt{2}$ . From the commutator  $[a, a^\dagger] = 1$  it follows,  $\forall z \in \mathbb{C}$ , that the coherent state

$$\psi_z := e^{-|z|^2/2} e^{za^\dagger} \psi_0 \quad (13)$$

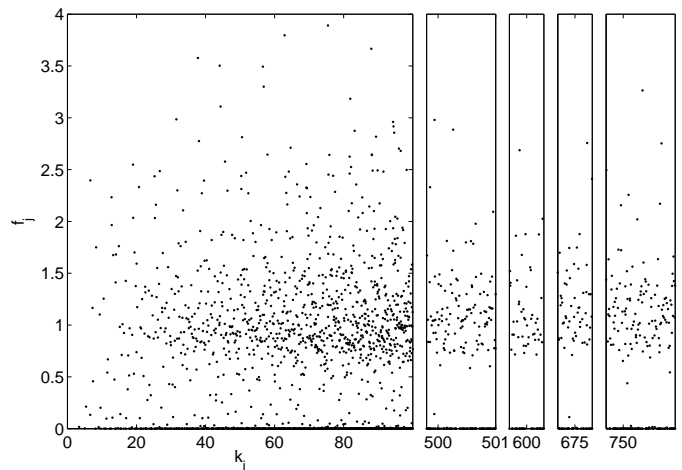


FIG. 12: Foot-sensing matrix elements  $f_j$  defined by (16), plotted vs  $k_j$ , for the complete set of odd modes with  $k_j < 100$  and smaller intervals at higher energy:  $499.8 < k_j < 501$ ,  $599.8 < k_j < 600.2$ ,  $674.8 < k_j < 675.2$  and  $749.8 < k_j < 750.6$  (there are 2316 total modes).

is an eigenfunction of  $a$  with eigenvalue  $z$ . The fact that it is  $L^2$ -normalized requires the Hermite-Gauss normalization  $\|(a^\dagger)^n \psi_0\|_2^2 = n!$ ,  $\forall n \in \mathbb{N}$ , which can be proved by induction. The Bargmann representation [43, 44] of a function  $v : \mathbb{R} \rightarrow \mathbb{C}$  is then  $\langle \psi_z, v \rangle$ ; the Husimi representation is its squared magnitude  $H_{v, \sigma}(z) := |\langle \psi_z, v \rangle|^2$ . We need a more explicit form than (13).  $\psi_z = e^{za^\dagger - z^* a} \psi_0$  follows by the Baker-Campbell-Hausdorff formula  $e^{A+B} = e^{-[A, B]/2} e^A e^B$  for  $[[A, B], A] = [[A, B], B] = 0$ . Applying this formula again and writing  $z := (q_0/\sigma + i\sigma k_0)/\sqrt{2}$  where  $q_0, k_0 \in \mathbb{R}$  gives

$$\psi_z(q) = e^{ik_0 q_0/2} e^{ik_0 q} \psi_0(q - q_0). \quad (14)$$

This shows that the coherent state is localized in position (around  $q_0$ ) and wavenumber (around  $k_0$ ), thus the Husimi is a microlocal (phase space) representation,

$$H_{v, \sigma}(q_0, k_0) := \left| \int_{-\infty}^{\infty} v(q) e^{ik_0 q} \psi_0(q - q_0) dq \right|^2. \quad (15)$$

This also known as the Gabor transform or spectrogram (windowed Fourier transform), and it can be proven equal to the Wigner transform convolved by the smoothing function  $\psi_0^2$ . Given a normal-derivative function  $\partial_n \phi_j$  we periodize it in order to apply the above. We also scale the wavenumber by  $k_j$ , thus the Birkhoff momentum coordinate is  $p = k_0/k_j$ . The choice of  $\sigma$  is somewhat arbitrary, but it is expected [45] that phase space structures have spatial scale  $O(k^{-1/2})$ , therefore we chose a scaling similar to this. At  $k = 500$  we used  $\sigma = 0.076$ .

In Fig. 11 we show boundary functions, their intensity, and Husimi distributions, for two modes. By comparing to the classical PSOS (Fig. 8), we see the first mode (the same as shown in Fig. 10) lives exclusively in the ergodic

phase space, whereas the second lives exclusively in regular phase space. In the first mode, the only large part of ergodic phase space not covered is that corresponding to bouncing-ball modes in the foot (the white ‘box’). Also a scar is visible as the 9 darkest spots: 4 pairs of spots surrounding the white box correspond to 4 bounces in the foot, and a single spot at  $q \approx 5$  corresponds to a normal-incidence bounce off the circular arc. This scar (as well as hints of other ones) is also somewhat visible in Fig. 10.

In Fig. 14 we show Husimi distributions for the 20 modes of Fig. 13; in the 19<sup>th</sup> the same scar discussed above is even more dominant. We remind the reader that in purely ergodic systems boundary functions obey the QET [25, 26] with almost every  $\partial_n \phi_j / k_j$  tending to an invariant Husimi density of the form  $C\sqrt{1-p^2}$ . We might expect a similar result to hold for the ergodic subset of modes in the ergodic phase space of the mushroom. However, Fig. 14 shows that despite being at a high mode number of roughly  $4 \times 10^4$  we are still a long way from reaching any invariant density: the 7 ergodic modes have highly nonuniform Husimi distributions.

## B. Fraction of regular modes

Finally we give more quantitative results on Percival’s conjecture. Since the PSOS phase space in  $0 < q < 3/2$  is ergodic for all  $p$ , we may use the  $L^2$  norm of the boundary function in this region as an indicator that a mode has an ergodic component. We define the ‘foot-sensing’ quadratic form

$$f_j := \int_0^{3/2} \left| \frac{\partial_n \phi_j(q)}{k_j} \right|^2 dq. \quad (16)$$

This may be thought of as the square of a diagonal matrix element of an operator which acts on boundary functions. Fig. 12 shows  $f_j$  vs  $k_j$  for the first 1746 odd modes (those discussed in Sec. IV) and a sample of 615 modes in the approximate range  $500 < k_j < 750$ . The highest shown correspond to mode number  $j \approx 10^5$ .

Percival’s conjecture would imply in the semiclassical limit the sequence  $\{f_j\}_{j=1 \dots \infty}$  has (for all but a set of vanishing measure) two limit points: zero (for regular modes), and some positive constant (for ergodic modes). Note that dividing by  $k_j$  as in (16) is necessary to scale the boundary functions so that matrix elements of a fixed operator can have a limit [25, 46]. The data shows a fraction of modes have  $f_j$  very close to zero and the rest have distribution around 1, whose width decreases somewhat as  $k_j$  increases; this supports the conjecture. Results on the rate of quantum ergodicity [18] lead us to expect slow convergence of such matrix elements in the ergodic region, even at high mode numbers of order  $10^5$ . This, combined with the long correlations in the ergodic dynamics, may explain why the nonzero  $f_j$  values have not reached anything like the constant value we would expect if the ergodic modes obeyed a QET.

We need to know the integrable phase space fraction  $\mu_{\text{int}}$ . The total phase space (restricting to the unit-speed momentum shell) has volume  $V_{\text{tot}} = \text{vol}(\Omega' \times S^1) = 2\pi \text{vol}\Omega' = 2\pi(ab/2 + \pi R^2/4)$ . Let us define the function  $\alpha(\mathbf{r}) := 2\pi - 4 \sin^{-1}(b/2d(\mathbf{r}))$ , where  $d(\mathbf{r})$  is the distance from  $\mathbf{r}$  to the center point  $q_c$ . When  $\mathbf{r}$  is a location in the hat for which  $d(\mathbf{r}) \in [b/2, R]$ , this function gives the measure of the set of angles in  $S^1$  for which orbits launched from  $\mathbf{r}$  are integrable (*i.e.* never leave the annulus  $d(\mathbf{r}) \in [b/2, R]$ ). The integrable phase space volume is found by integrating  $\alpha(\mathbf{r})$  over this annulus, for which we use polar coordinates  $(\rho, \phi)$  with origin at  $q_c$ . Thus, we calculate,

$$\begin{aligned} V_{\text{int}} &= \int_0^{\pi/2} d\phi \int_{b/2}^R \alpha(\rho) \rho d\rho \\ &= \frac{\pi^2}{2} \left( R^2 - \frac{b^2}{4} \right) - 2\pi \int_{b/2}^R \rho \sin^{-1} \frac{b}{2\rho} d\rho \\ &= 2\pi \left( \frac{\pi}{4} R^2 - \frac{bR\rho_0}{4} - R \sin^{-1} \frac{b}{2R} \right). \end{aligned}$$

For our shape this gives  $\mu_{\text{int}} = V_{\text{int}}/V_{\text{tot}} = 0.3987 \dots$

We categorize modes by calling them regular if  $f_j < 10^{-2}$ . The choice of this cut-off is somewhat arbitrary, however in the  $j \rightarrow \infty$  limit it should become irrelevant. Counting all 2361 odd modes in Fig. 12 we have 977 regular ones, thus a fraction  $0.414 \pm 0.01$  (here the standard error assumes a model in which each mode independent Bernoulli trial). To give an idea of reliability of this figure, a cut-off of  $10^{-1}$  gives 0.434, and a cut-off of  $10^{-3}$  gives 0.398; smaller values start to be affected by numerical errors in modes. If we restrict to the 615 high modes  $k_j > 499.8$ , the fraction is  $0.441 \pm 0.02$ , almost independent of any reasonable cut-off choice. This would lead one to reject the null hypothesis that the underlying probability of any mode being regular is  $\mu_{\text{int}}$ , with  $p$ -value 0.04, not a very significant deviation. Thus, the observed regular fraction is reasonably consistent with (within 2 standard errors of) the conjectured value of  $\mu_{\text{int}}$ .

## VI. CONCLUSION

We have presented the first known high-lying eigenmode calculations of Bunimovich’s mushroom domain, which has a simple divided phase space without KAM hierarchy. Using a basis set adapted to the re-entrant corner, the Method of Particular Solutions achieves very high accuracy for low modes, and the scaling method enables us to find high modes orders of magnitude more efficiently than any other known numerical approach. We find strong numerical evidence that Percival’s conjecture is satisfied, and with the two mode types occurring with frequencies given by their invariant phase space volumes. Without doubt this result could be strengthened using a more selective phase-space measure and by collecting

more statistics. We note that if a quantum ergodicity result is to hold for the ergodic subset of modes, we are far from having reached this regime despite being at mode numbers in the tens of thousands. This slow convergence to quantum ergodicity has been studied in detail in completely ergodic systems [18].

This study is by necessity preliminary, and many questions remain. What is the level-spacing distribution? What are the spectral manifestations of stickiness [10, 11]? On the numerical methods side there remain many open issues [18, 31, 32], and a probable order of

magnitude speed-up possible due to the currently slow evaluation of high-order Bessel functions.

### Acknowledgments

We thank Mason Porter, Eric Heller and Nick Trefethen for stimulating discussions. AHB is partially funded by NSF grant DMS-0507614.

- 
- [1] L. A. Bunimovich, *Chaos* **11** (2001).
- [2] I. C. Percival, *J. Phys. B* pp. L229–232 (1973).
- [3] M. C. Gutzwiller, *Chaos in classical and quantum mechanics*, vol. 1 of *Interdisciplinary Applied Mathematics* (Springer-Verlag, New York, 1990).
- [4] S. De Bièvre, in *Second Summer School in Analysis and Mathematical Physics (Cuernavaca, 2000)* (Amer. Math. Soc., Providence, RI, 2001), vol. 289 of *Contemp. Math.*, pp. 161–218.
- [5] S. Zelditch, in *Elsevier Encyclopedia of Mathematical Physics* (Elsevier, 2006), to appear, <http://arxiv.org/math-ph/0503026>.
- [6] Y. G. Sinai, *Uspehi Mat. Nauk* **25**, 141 (1970).
- [7] L. A. Bunimovich, *Chaos* **1**, 187 (1991).
- [8] Y. G. Sinai, *Notices Amer. Math. Soc.* **51**, 412 (2004).
- [9] M. A. Porter and S. Lansel, *Notices Amer. Math. Soc.* **53**, 334 (2006).
- [10] E. G. Altmann, A. E. Motter, and H. Kantz, *Chaos* **15**, 033105, 7 (2005), <http://arxiv.org/nlin.CD/0502058>.
- [11] E. G. Altmann, A. E. Motter, and H. Kantz, *Physical Review E (Statistical, Nonlinear, and Soft Matter Physics)* **73**, 026207 (pages 10) (2006), URL <http://link.aps.org/abstract/PRE/v73/e026207>.
- [12] J. R. Kuttler and V. G. Sigillito, *SIAM Rev.* **26**, 163 (1984).
- [13] A. Dhar, D. Madhusudhana Rao, U. Shankar N., and S. Sridhar, *Phys. Rev. E* (3) **68**, 026208, 5 (2003).
- [14] G. Vidmar, Master’s thesis, Ljubljana, Slovenia (2005), available at <http://www-f9.ijs.si/~krizan/sola/sempod/0405/vidmar.pdf>.
- [15] A. Bäcker, in *The mathematical aspects of quantum maps* (Springer, Berlin, 2003), vol. 618 of *Lecture Notes in Phys.*, pp. 91–144.
- [16] E. Vergini and M. Saraceno, *Phys. Rev. E* **52**, 2204 (1995).
- [17] A. H. Barnett, Ph.D. thesis, Harvard University (2000), available at <http://www.math.dartmouth.edu/~ahb/thesis.html/>.
- [18] A. H. Barnett, *Comm. Pure Appl. Math.* **59**, 1457 (2006).
- [19] E. Lindenstrauss, *Ann. of Math.* (2) **163**, 165 (2006).
- [20] F. Faure, S. Nonnenmacher, and S. De Bièvre, *Comm. Math. Phys.* **239**, 449 (2003).
- [21] A. I. Schnirelman, *Usp. Mat. Nauk.* **29**, 181 (1974).
- [22] Y. Colin de Verdière, *Comm. Math. Phys.* **102**, 497 (1985).
- [23] S. Zelditch, *Duke Math. J.* **55**, 919 (1987).
- [24] S. Zelditch and M. Zworski, *Comm. Math. Phys.* **175**, 673 (1996).
- [25] A. Hassell and S. Zelditch, *Comm. Math. Phys.* **248**, 119 (2004).
- [26] A. Bäcker, S. Fürstberger, and R. Schubert, *Phys. Rev. E* (3) **70**, 036204, 10 (2004).
- [27] J. Marklof and S. O’Keefe, *Nonlinearity* **18**, 277 (2005).
- [28] G. Carlo, E. Vergini, and A. J. Fendrik, *Physical Review E (Statistical Physics, Plasmas, Fluids, and Related Interdisciplinary Topics)* **57**, 5397 (1998), URL <http://link.aps.org/abstract/PRE/v57/p5397>.
- [29] C. B. Moler and L. E. Payne, *SIAM J. Numer. Anal.* **5**, 64 (1968).
- [30] J. R. Kuttler and V. G. Sigillito, *SIAM J. Math. Anal.* **9**, 768 (1978).
- [31] A. H. Barnett, *Improved inclusion of dirichlet eigenvalues via perturbation theory on the boundary*, in preparation.
- [32] T. Betcke, *The generalized singular value decomposition and the method of particular solutions* (2006), preprint, submitted to *SIAM J. Sci. Comp.*
- [33] E. J. Heller, in *Chaos et physique quantique (Les Houches, 1989)* (North-Holland, Amsterdam, 1991), pp. 547–664.
- [34] P. R. Garabedian, *Partial differential equations* (John Wiley & Sons Inc., New York, 1964).
- [35] L. Fox, P. Henrici, and C. Moler, *SIAM J. Numer. Anal.* **4**, 89 (1967).
- [36] T. Betcke and L. N. Trefethen, *SIAM Rev.* **47**, 469 (2005).
- [37] M. Galassi *et al.*, *GNU Scientific Library Reference Manual*, <http://www.gnu.org/software/gsl/>.
- [38] A. R. Barnett, D. H. Feng, J. W. Steed, and L. J. B. Goldfarb, *Comput. Phys. Commun.* **8**, 377 (1974).
- [39] W. H. Press, S. A. Teukolsky, W. T. Vetterling, and B. P. Flannery, *Numerical recipes in C* (Cambridge University Press, Cambridge, 2002).
- [40] F. Rellich, *Math. Z.* **46**, 635 (1940).
- [41] A. H. Barnett, *Migrating fringes of scars in mushrooms and other billiards*, in preparation.
- [42] J.-M. Tualle and A. Voros, *Chaos Solitons Fractals* **5**, 1085 (1995).
- [43] V. Bargmann, *Comm. Pure Appl. Math.* **14**, 187 (1961).
- [44] V. Bargmann, *Comm. Pure Appl. Math.* **20**, 1 (1967).
- [45] E. J. Heller, *Phys. Rev. Lett.* **53**, 1515 (1984).
- [46] A. Bäcker, S. Fürstberger, R. Schubert, and F. Steiner, *J. Phys. A* **35**, 10293 (2002).
- [47] J. Rauch, *Amer. Math. Monthly* **85**, 359 (1978).
- [48] S. A. Fulling and P. Kuchment, *Inverse Problems* **21**,

1391 (2005).

[49] We note that a related Penrose-Lifshits mushroom construction [47] continues to find use in isospectral prob-

lems [48]

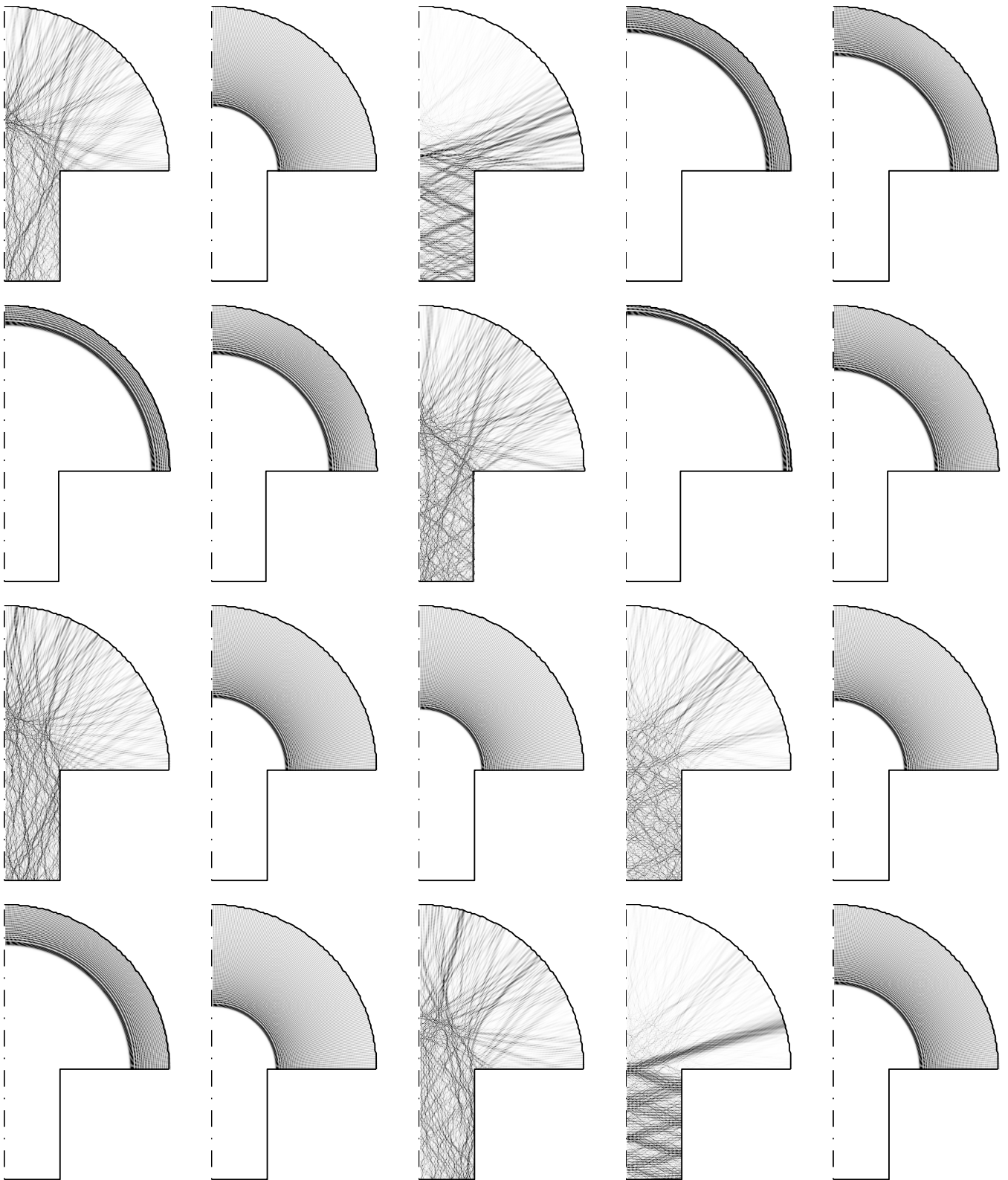


FIG. 13: 20 high-eigenvalue modes with consecutive eigenvalues, covering the range  $k_j \in [499.800, 499.869]$ , with mode number around  $j \approx 45000$ . Mode number increases horizontally from the top left.  $|\phi_j|^2$  is shown with zero white and larger values darker.

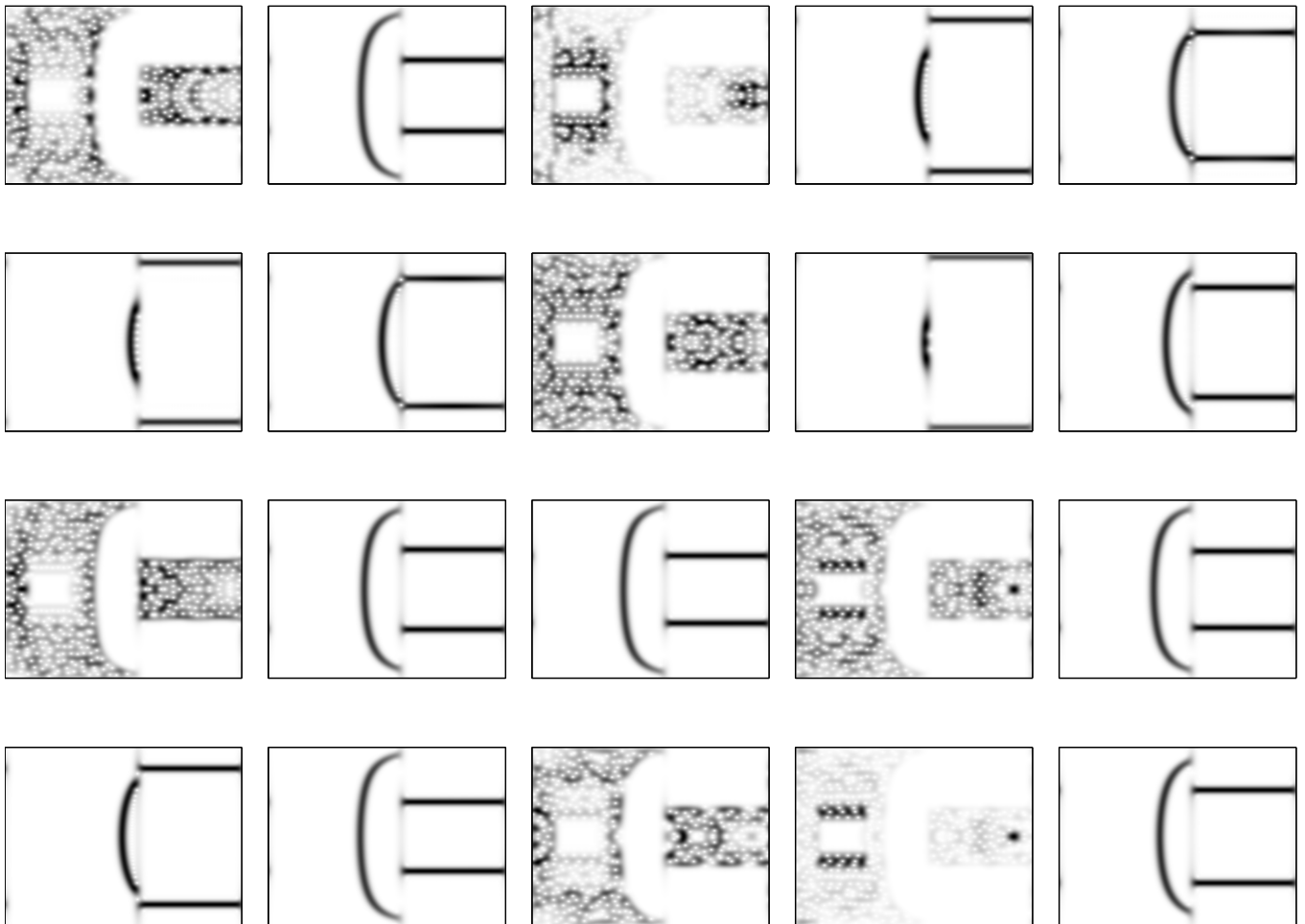


FIG. 14: Husimi distributions  $H_{\partial_n, \phi_j, \sigma}(q, p)$  of the 20 high-eigenvalue modes shown in Fig. 13, in the same order. The  $q$  and  $p$  axes are as in Fig. 11.